Mitragyna speciosa Alkaloids Inhibit Proliferation and Metastasis in Luminal A and Triple-Negative Breast Cancer Mediated by AKT1 and Mortalin

Anissa Nofita Sari
anis032@brin.go.id
National Research and Innovation Agency
Dwi Wahyu Indriani
National Research and Innovation Agency
Siti Irma Rahmawati
National Research and Innovation Agency
Asep Bayu
National Research and Innovation Agency
Gayathri Sundaram
BIONYERI Pty Ltd
Umut Rende
BIONYERI Pty Ltd
Gilles J. Guillemin
BIONYERI Pty Ltd
Peni Ahmadi
National Research and Innovation Agency
Bustanussalam Bustanussalam
National Research and Innovation Agency
Yatri Hapsari
National Research and Innovation Agency
Ni Luh Putu Indi Dharmayanti
National Research and Innovation Agency
Masteria Yunovilsa Putra
National Research and Innovation Agency

Research Article

Keywords: Kratom alkaloids, Luminal A, Triple-Negative Breast Cancer (TNBC), AKT1, mortalin

Posted Date: January 6th, 2026

DOI: https://doi.org/10.21203/rs.3.rs-8421744/v1

Additional Declarations: No competing interests reported.

Abstract

Breast cancer, including subtypes luminal A and triple-negative breast cancer (TNBC), presents considerable clinical challenges due to its heterogeneity and resistance to current treatments. This highlights an urgent need for new therapeutic strategies targeting multiple oncogenic pathways. This study assessed the anti-cancer efficacy of kratom (*Mitragyna speciosa*) alkaloids on Luminal A (MCF-7) and TNBC (MDA-MB-231) cell lines. We evaluate the potential anticancer capacities of kratom alkaloids using a combination of network pharmacology, molecular docking, and dynamics, alongside *in vitro* and molecular experiments. This multilevel approach focused on assessing the effects on proliferation, migration, invasion, and cell cycle, as well as on identifying the underlying molecular targets. Kratom alkaloids markedly decreased cellular proliferation, induced G2/M phase arrest, and suppressed tumoral metastasis-associated capacities. These effects were mediated by the downregulation of AKT1 and mortalin (HSPA9), leading to the reactivation of p53 signalling. Molecular docking validated robust binding affinities of alkaloids to both targets. The Cancer Genome Atlas (TCGA) analysis corroborated the alkaloids clinical significance in breast cancer. The results highlight a significant therapeutic potential for Kratom alkaloids as dual-target medicines demonstrating both anti-proliferative and anti-metastatic effects in Luminal A and TNBC models.

Background

Breast cancer has become a major challenge worldwide due to its high incidence, biological complexity, and increasing resistance to existing treatment regimens. It constitutes 11.6% of global cancer cases and 24.2% of cancer cases in women (1), with approximately 2.3 million new diagnoses annually, making it the most commonly diagnosed cancer and a leading cause of cancer-related mortality (2). Breast cancer is categorized into molecular subtypes based on the expression of estrogen receptor (ER), progesterone receptor (PR), and human epidermal growth factor receptor 2 (HER2) (3) (4), which significantly influences clinical behavior and treatment response. Tumours expressing both ER and PR are classified as hormone receptor-positive and typically respond well to hormone therapy (5), whereas HER2 overexpression is associated with increased tumour aggressiveness, diminished efficacy of hormone therapy, and often requires specialized treatment strategies (6). Luminal A cancers are characterized by ER or PR positivity, HER2 negativity, and low Ki-67 expression, rendering them less aggressive and highly responsive to hormone therapy (7) (8). However, relapse occurs in 30–50% of cases due to tumour dormancy, late metastasis progression (9) (10), and therapeutic resistance (11). In contrast, Triple-Negative Breast Cancer (TNBC), which lacks ER, PR, and HER2 expression, displays elevated proliferative activity, leading to a more aggressive phenotype, poor prognosis (12), frequent metastasis, and treatment resistance, highlighting the urgent need for tailored and personalized therapeutic strategies.

Beyond receptor expression, breast cancer progression is also shaped by dysregulated molecular pathways, including the PI3K/AKT signalling axis (13) (14) and mitochondrial chaperones such as HSPA9 (also known as mortalin) (15) (16). AKT1, a serine/threonine kinase that regulates cell

proliferation, survival, metabolism, and metastatic potential (17) (18), and is frequently hyperactivated in breast cancer, is associated with poor prognosis and chemotherapy resistance (19). This pattern is further supported by clinical evidence showing that elevated p-AKT1 expression correlates with lower survival rates and treatment efficacy (20). Likewise, mortalin, a mitochondrial heat shock protein involved in protein homeostasis and cellular stress responses (21), is overexpressed in multiple malignancies and contributes to enhanced tumorigenicity, proliferation, metastasis, and invasion (22) (23). Together, the pivotal roles of AKT1 and mortalin in malignant progression underscore their potential as powerful therapeutic targets for improving clinical outcomes in breast cancer.

Despite advances in targeted therapies and personalized medicine, therapeutic resistance continues to cause elevated relapse rates and poor clinical outcomes, particularly in aggressive subtypes like TNBC, underscoring the need for novel therapeutic strategies. Natural products remain important sources of anticancer agents due to their structural diversity and bioactivity (24) (25). Kratom (*Mitragyna speciosa*), a traditional herbal remedy indigenous to Southeast Asia, contains bioactive alkaloids with reported anti-inflammatory, analgesic, antioxidant (26), and anticancer properties, such as apoptosis-mediated inhibition of A459 human lung cancer cell growth (27). However, the anticancer potential of kratom-derived alkaloids in Luminal A and TNBC remains unexplored. This study hypothesizes that kratom-derived alkaloids can modulate breast cancer progression by targeting AKT1 and Mortalin pathways. It further aims to elucidate the underlying mechanisms of the anticancer effects using an integrated approach combining network pharmacology, molecular docking, and *in vitro.* The findings are expected to advance phytotherapeutics research and offer a scientific basis for developing natural product-based anticancer therapies.

Material and methods

Sample Preparation

Mitragyna speciosa (kratom) crude and alkaloid extracts were prepared following the pilot-scale extraction protocol (100 L capacity), which we previously reported (27) without any modifications. The crude extracts were obtained through methanolic extraction of dried kratom leaves. The alkaloid-rich extract was subsequently prepared using an acid-base fraction process applied to the crude extract, as detailed in the earlier report. To ensure extract quality and consistency, purity and alkaloid composition were verified using HPLC chromatographic profiling. In accordance with the value, the crude extract contained approximately 4.5–50% mitragynine (MG), whereas the alkaloid extract exhibited an MG content of 38–46% (27). These validated batches were exclusively used in the present study.

Cell Culture and Reagents

The Luminal-A (MCF-7), Triple-Negative Breast Cancer (MDA-MB-231) cell lines and normal cells (HEK29T3) were purchased from (European Collection of Authenticated Cell Cultures (ECACC) and were

maintained in low-glucose Dulbecco's Modified Eagle's Medium (DMEM) (Sigma Aldrich, ST. Louis, MO, USA) supplemented with L-glutamine, phenol red, 1% of antibiotic and antimycotic solution 100× (Sigma Aldrich, ST. Louis, MO, USA), and 5–10% fetal bovine serum (v/v) (Sigma Aldrich, ST. Louis, MO, USA). Cells were incubated at 37°C in a humidified atmosphere containing 5% CO_2.

Cell Viability Assay

The colorimetric method, using 3-(4,5-dimethylthiazol-2-yl)-2,5-diphenyltetrazolium bromide (MTT, Sigma-Aldrich, Burlington, MA, USA), was employed to indirectly assess cell viability by measuring mitochondrial enzymatic activity. 5000 cells were seeded in 100 µL of complete medium in each of the 96 wells and incubated for 24 hours at 37°C in 5% CO_2 and humidity. After the 24-h attachment period, the medium was replaced with fresh medium containing the extract, and cells were incubated for an additional 24 or 48 hours. The percentage of cell viability was determined by comparing the viability of cells treated with Kratom extract and those that were untreated.

Colony formation assay

In six-well plates, 500 cells per well were plated and left to adhere overnight. After this time of incubation, control media, kratom alkaloids, or kratom crude (0.0020; 0.020 mg/mL) were added to the cells. Colonies were allowed to form over 10 to 14 days, with medium replaced every 3 days.

In Vitro Scratch Assay

MCF-7 and MDA-MB-231 cells (1 × 10^5 cells/well) were seeded in six-well plates and incubated overnight at 37°C in a CO_2 incubator to form monolayers. Using a p200 pipette tip, the cell monolayer was gently scraped to create a linear wound. Following three PBS washes, the cells were cultivated in either the control culture medium or test conditions containing the extract. The speed of cell migration was monitored and recorded using a microscope (Olympus CKX53).

The Transwell Migration Assay

We used a transwell system to assess the migration capacity of MCF-7 and MDA-MB-231 cells in the absence of Matrigel coating. The upper chamber of a 24-well Transwell insert (8 µm pore size, Corning Inc., USA) was filled with 0.5 mL of serum-free DMEM containing the cancer cells. The lower chamber was filled with 0.75 mL of DMEM supplemented with 10% fetal bovine serum (FBS) as a chemoattractant. Non-migrating cells on the upper side of the membrane were delicately removed using a cotton swab after 48 hours of incubation at 37°C in a 5% CO_2 atmosphere. The vehicle control consisted of cells treated with DMSO.

Transwell Invasion Assay

Matrigel-coated transwell chambers (Corning BioCoat Matrigel Invasion Chamber, Product No: 354480) were employed to evaluate cell invasion capacity. MCF-7 and MDA-MB-231 cells were resuspended in 0.5 mL of serum-free DMEM and transferred into the upper compartment of the Matrigel-coated inserts. As a chemoattractant, 0.75 mL of DMEM containing 10% FBS was added to the lower wells of the 24-well plate. The inserts were meticulously rinsed with phosphate-buffered saline (PBS) after 48 hours of incubation at 37°C with 5% CO_2.

Cell Cycle Assay

The cell cycle of MCF-7 and MDA-MB-231 cells was quantified using 4',6-diamidino-2-phenylindole (DAPI) staining (C001 ABP Bioscience) to investigate the distribution of cell cycle phases. Under conventional culture conditions, cells were seeded into a black-wall 96-well Black/Clear Bottom plate at a density of 10,000 cells per well and allowed to adhere for 24 hours. The nuclear DNA was stained by incubating the cells with 1 µg/mL DAPI solution for 5 minutes in the dark at room temperature after treatment or incubation as required. The cells were fixed with 4% paraformaldehyde and rinsed three times with PBS to remove excess dye. Cells were categorized into the G1, S, and G2/M phases based on their fluorescence intensity.

Target Gene Identification

The identification of a target gene for breast cancer was conducted using a network pharmacology approach that integrates biological and pharmacological systems. Data mining was performed using six major breast cancer-related gene databases, including GeneCards, OMIM, PharmGKB, STRING, CTD, and The Human Protein Atlas. Compound-related genes were obtained from SEA search, Swiss Target Prediction, Binding DB, and CTD. Intersection analysis was performed using Venny 2.1.

GO and KEGG enrichment analysis

The best gene candidates were re-validated based on biological processes using Metascape and SRplot. Metascape was used for gene ontology (GO) identification, based on several existing databases, including Disgenet, TRRUST, and transcription factor targets. Cross-validation with SRplot was performed to examine biological processes, cellular components, and molecular functions. SRplot also facilitates the overall KEGG enrichment analysis, along with the identification of the best pathways within the gene pool used.

The Cancer Genome Atlas (TCGA) Analysis

As a final validation for the selection of potential gene targets, cross-validation was carried out using the UALCAN TCGA. This analysis was used only to retrieve mRNA expression profiles and survival

information of the selected gene candidates based on the TCGA breast cancer datasets, and the detailed interpretation of these findings is presented in the results section.

RNA Extraction

Total RNA was extracted from MCF-7 and MDA-MB-231 cell pellets utilizing TRIzol™ Reagent (Invitrogen, Thermo Fisher Scientific, USA) according to the manufacturer's instructions. After homogenization in TRIzol, the aqueous RNA phase was collected following phase separation with chloroform. RNA precipitation was performed using isopropanol, followed by washing with 75% ethanol. The RNA pellet was air-dried, reconstituted in RNase-free water, and quantified using a NanoDrop™ spectrophotometer. The extracted RNA was preserved at − 80°C for subsequent qRT-PCR analysis.

Quantitative Real-Time Polymerase Chain Reaction

Quantitative reverse transcription PCR (qRT-PCR) was performed using the HiScript II One Step qRT-PCR SYBR Green Kit (Vazyme, Cat. No. Q221-01), which enables reverse transcription and amplification in a single step. Each 20 µL reaction mixture comprised 10 µL of RNase-free water, 1 µL of 2× One Step SYBR Green Mix, 0.4 µL of One Step SYBR Green Enzyme Mix, and 0.4 µL of 50× ROX Reference. Combine 1 µL of template RNA with 0.4 µL of forward primer (10 µM) and 0.4 µL of reverse primer (10 µM). All reagents were produced under RNase-free conditions, and reactions were conducted in triplicate. The sequences of forward and reverse primers can be found in Supplementary Table 1. Gene expression levels were assessed via the ΔΔCt technique, normalized to internal control genes.

Immunocytochemistry and High-Content Imaging Analysis

MCF-7 and MDA-MB-231 cells were seeded in black 96-well plates or 24-well plates and allowed to adhere overnight, followed by treatment with kratom alkaloid and kratom crude for 48 hours. After treatment, cells were rinsed with PBS, fixed with 4% PFA, permeabilized with Triton X-100, and blocked with 5% Bovine Serum Albumin (BSA). Cells were incubated with primary antibodies targeting MMP-3, Ki-67, p53, MMP-9, HSPA9, and AKT, followed by appropriate fluorophore-conjugated secondary antibodies. Nuclear counterstaining was performed using DAPI, and fluorescence imaging was acquired using the CellInsight™ CX7 LZR Pro High Content Screening System (Thermo Fisher, Scientific). Quantitative fluorescence analysis was performed using HCS Studio 5.0 Cell Examination Software.

Molecular Docking

Molecular docking simulations were performed using AutoDock Vina to evaluate the interaction between the Kratom-derived candidate compounds and the target proteins AKT1 and Mortalin. Binding affinity values and RMSD were used to assess docking quality, and docking interactions were further examined using Biovia Discovery Studio and PyMol.

Molecular Dynamics

Molecular dynamics simulations were carried out using a combination of CHARMM-GUI and GROMACS. The preparation stage was carried out using CHARMM-GUI, including topology preparation, minimization,

and equilibration. The parameters used include temperature 310K, NaCl concentration (0.1%), Amber force field, and time for 100 ns. GROMACS was used to simulate molecular dynamics by performing the stages of minimization, equilibration, and dynamics simulation. Visualization of the results was done using xmgrace to see the trajectory of the file in the form of rmsd, rmsf, hydrogen bond, and radius of gyration.

Statistical Analysis

Three or more data are presented as the mean ± standard deviation (SD). Statistical analyses and all graphs were generated using OriginPro 2019 software (OriginLab, Japan). Data were analyzed using a two-sample t-test to compare each treatment group with its corresponding control, or by one-way analysis of variance (ANOVA), followed by Tukey's post hoc test. A p-value < 0.05 was considered statistically significant.

Results

Kratom alkaloids exhibit superior anti-proliferative and clonogenic inhibitory effects compared to crude extract in MCF-7 and MDA-MB-231 cells

To analyse the cytotoxic effect of kratom crude extract (KC) and alkaloid-enriched fraction (KA), MTT assay was conducted on MCF-7 and MDA-MB-231 breast cancer cells treated with a dosage range of 0.003 to 0.2 mg/mL. Figure 1A and 1B show that both extracts lower cell viability in a concentration-dependent manner. However, the alkaloid fraction showed a stronger effect in both cell lines. The alkaloid fraction was nearly three times more effective than the crude extract, as evidenced by the IC_{50} values of KC of 0.071 mg/mL and 0.12 mg/mL, while the IC_{50} values for KA were 0.023 mg/mL and 0.022 mg/mL in MCF-7 and MDA-MB-231 cells, respectively.

The efficacy of kratom extracts was further examined using a clonogenic assay. As shown in Fig. 1C and 1D, both MCF-7 and MDA-MB-231 cells exhibited a significant reduction in colony formation in the presence of KA and KC, even at low concentrations. Treatment with 0.01 mg/mL KA or KC nearly halted colony formation in MCF-7 cells ($p = 0$) and inhibited colony growth by almost 90% in MDA-MB-231 cells ($p = 0$). At 0.005 mg/mL, KC decreased colonies by roughly 70% ($p = 0$), whereas KA induced about a 50% reduction ($p = 0$) in MCF-7 cells. In MDA-MB-231 cells, both KA and KC reduced colony number by approximately 70% ($p = 0$). These results indicate that both crude extract and alkaloid fraction reduced clonogenic survival, with the alkaloid fraction showing higher effectiveness, in line with the IC_{50} results.

Cytotoxicity was also evaluated in normal human embryonic kidney cells (HEK-293) (Supplementary Fig. 1). The crude extract exhibited little toxicity, with high IC_{50} values of 2.14 mg/mL at 24 h and 3.283 mg/mL at 48 h, and cell viability remained close to baseline across the tested concentration range. In contrast, the alkaloid fraction showed different effects, with HEK-293 viability decreasing at much lower doses, as reflected by lower IC_{50} values of 0.051 mg/mL and 0.034 mg/mL. To assess whether this translated into selectivity toward tumour cells, the Selectivity Index was calculated. At 24 hours, the

alkaloid fraction showed moderate selectivity (SI ~ 2.2–2.3), but this was no longer observed at 48 hours (SI < 2). In contrast, the crude extract showed consistently high SI values (17–46), indicating better sparing of normal cells while retaining anticancer activity. Thus, although the alkaloid-rich fraction is more potent, the crude extract appears to offer a wider safety margin.

Kratom alkaloids inhibit the cell cycle of breast cancer cells through G2/M phase arrest.

MTT and clonogenic assays showed that kratom alkaloids are more inhibitory compared to crude extracts. Based on this result, we investigated the effect of kratom alkaloids on the cell cycle. After 48 hours of DAPI staining, cell cycle analysis was conducted in MCF-7 and MDA-MB-231 cells to study the mechanism of the anti-proliferative activity of kratom alkaloids. Figure 1E-F demonstrates that kratom alkaloids induce G2/M-phase arrest in both cell lines, with the highest G2/M accumulation observed at a concentration of 0.048 mg/mL ($p = 0$ in MCF-7 and MDA-MB231 groups). All tested concentrations also increased the S-phase population in both cells, with the greatest increase observed at a concentration of 0.024 mg/mL ($p < 0.001$ vs. other concentrations). A concentration-dependent rise in the G0/G1 phase was also observed in both cells, starting at 0.024 mg/mL ($p = 0$) and becoming more pronounced at 0.048 mg/mL ($p < 0.001$). Overall, these data, together with the MTT and clonogenic data, demonstrate that both breast cancer cell types respond similarly to Kratom treatment, with the alkaloid fraction showing stronger activity, particularly in hormone receptor–positive MCF-7 cells, as indicated by their greater reduction in viability compared to MDA-MB-231 cells (Fig. 1A-B).

Kratom alkaloids inhibit the invasion and migration of breast cancer cells

The anti-metastatic effects of kratom alkaloids were evaluated using wound-healing scratch assays and transwell assays. In both MCF-7 and MDA-MB-231 cells, treatment with alkaloid extract slowed migration in the scratch assay (Fig. 2A–B). In MCF-7 cells, exposure to 0.006 or 0.012 mg/mL kratom alkaloid reduced wound closure at 24–48 hours (Fig. 2A), while MDA-MB-231 cells showed delayed wound closure between 48 and 72 hours (Fig. 2B). The higher percentage of uncovered area indicates that alkaloid extracts inhibit cell migration. Scratch assays performed with the crude extract showed a similar inhibitory pattern at the same time points (0, 24, 48, and 72 h) (Supplementary Fig. 2A and 2B).

To further support these observations, transwell migration assays were performed (Fig. 2C and 2D). Kratom alkaloids reduced the number of migrating cells in a concentration-dependent manner. In MCF-7 cells, migration was significantly decreased at 0.006 and 0.012 mg/mL ($p = 0$ for both concentrations compared to the control group; Fig. 2C). Similar effects were observed in MDA-MB-231 cells, where both concentrations lowered cell migration relative to the control. Invasive behaviour was next examined using Matrigel-coated transwell inserts (Fig. 2E and 2F). Both cell lines showed reduced invasion following alkaloid treatment. In MCF-7 cells, concentrations of 0.006 and 0.012 mg/mL decreased invasion to approximately 60% of the untreated group ($p < 0.001$ for both concentrations; Fig. 2E). MDA-MB-231 cells showed a stronger response, with the highest dose (0.012 mg/mL) nearly abolishing

invasion ($p < 0.001$; Fig. 2F). Together, these data indicate that kratom alkaloids inhibit both migration and invasion in breast cancer cells, including hormone receptor-positive and triple-negative lines.

Kratom alkaloid target, hub genes, and biological functions revealed by Network Pharmacology

We integrated LC–MS/MS data that were previously reported (27–29) with literature-curated compounds (30) to identify candidate genes using a network pharmacology-based approach, aiming to explore the molecular mechanisms underlying the anticancer effects of kratom alkaloids (Fig. 3A). From 167 kratom-related targets and 1115 breast cancer–related genes, 49 overlapping genes were identified (Fig. 3B). These genes were analysed using topological filtering and protein–protein interaction (PPI) network construction, revealing 49 interacting nodes (Fig. 3C, left). A high-confidence subnetwork of 20 genes was extracted based on degree (> 40), betweenness centrality (> 0.005), and clustering coefficient (> 0.6) (Fig. 3C, middle). Further selection using oncogene classification, availability of structural models in the RCSB database, and literature relevance identified nine core genes: *AKT1, EGFR, CCND1, ERBB2, MTOR, MAPK1, PIK3CA, CDK4*, and *CDK2* (Fig. 3C, right). Metascape enrichment analysis of the 49 genes revealed enrichment in cancer-related biological processes and pathways (Fig. 3D), with prominent terms including ‘positive regulation of small molecule metabolic process’, ‘response to xenobiotic stimulus’, ‘cellular response to lipid’, and ‘hormone metabolic process’. These processes are linked to metabolic adaptation and xenobiotic handling in cancer cells, suggesting that kratom alkaloids may influence cancer metabolism and intracellular signalling. Consistently, enrichment of ‘microRNAs in cancer’, ‘MAPK signalling’, and the ‘PI3K–AKT pathway’ reflected established roles of AKT1, MTOR, and related genes. Gene Ontology grouping further showed that the same nine targets were involved in pathways associated with proliferation, migration, and metastasis (Fig. 3E), including ‘positive regulation of cell migration’ and ‘regulation of cell proliferation’. Scoring analysis based on network centrality and functional relevance ranked AKT1 and EGFR highest (score = 74), followed by CCND1 (score = 68) and ERBB2 (score = 58). Given the frequent upregulation of AKT1 in breast cancer and its role in survival signalling, its identification as a major network hub is biologically relevant. Overall, these findings indicate that kratom alkaloids may act on multiple cancer-related targets, collectively modulating pathways involved in proliferation, migration, and survival in breast cancer.

Inhibition of AKT1 expression and associated oncogenes by kratom alkaloids in breast cancer cells

According to network pharmacology analysis (Fig. 3), AKT1 was identified as the highest-ranked hub gene, together with other oncogenic regulators such *as EGFR, CCND1, ERBB2, MTOR, MAPK1, PIK3CA, CDK4*, and *CDK2*, which are frequently associated with the PI3K/AKT signalling pathway (31) (32). Functional annotation and KEGG enrichment showed that these targets cluster within major cancer-related signalling modules (Supplementary Figs. 3 and 4). TCGA-based expression and survival analysis using the UALCAN platform demonstrated that AKT1, HSPA9, and CCND1 were overexpressed in breast tumour tissues compared with normal samples. However, only HSPA9 overexpression was significantly

associated with poorer overall survival (p = 0.01), whereas AKT1 and CCND1 showed no significant prognostic impact (p = 0.44 and p = 0.21, respectively; Supplementary Fig. 5). Thus, HSPA9 emerged as the most clinically informative target, while AKT1 and CCND1 remained frequently elevated oncogenic candidates requiring experimental validation.

To validate these predictions, qRT–PCR and immunofluorescence analyses were performed to examine transcript and protein expression following kratom alkaloid treatment. Treatment with kratom alkaloids (0.014 mg/mL) significantly reduced mRNA levels of *AKT1, EGFR, CCND1, ERBB2, MTOR, MAPK1, PIK3CA*, *and CDK2* in both MCF-7 and MDA-MB-231 cells compared with untreated controls (Fig. 4A, B). These results are consistent with pathway enrichment analysis and the network-based prioritisation of AKT1. Immunofluorescence quantification and high-content protein analysis further revealed a significant reduction in total AKT1 protein expression in both cell lines ($p < 0.001$) (Figs. 4C and D, Supplementary Fig. 6). Cytoplasmic AKT1 signals were reduced after kratom alkaloid treatment, and MCF-7 cells showed changes in the nuclear–cytoplasmic distribution of AKT1. In line with the qRT–PCR results, AKT1 expression was decreased at both the transcript and protein levels, supporting its involvement as a major target identified through network pharmacology and TCGA analyses.

Molecular docking and molecular dynamics simulations indicate structurally plausible binding of kratom Alkaloids to AKT1

AKT1 emerged as a major node from both the network analysis and the expression data, so we examined whether any of the kratom alkaloids might physically fit into its binding pocket. In the docking study, ajmalicine and speciociliatine repeatedly appeared as the most compatible ligands, with predicted binding energies of − 11.1 kcal/mol and − 10.0 kcal/mol. These values were weaker (around − 14.4 kcal/mol) than the affinity of the co-crystallised AKT1 inhibitor (Fig. 4E, F; Supplementary Fig. 12; Supplementary Table 2), but both alkaloids still located themselves in a clear pocket region. The docked poses interacted with several residues often observed in AKT1–ligand interactions, including Leu264, Asp292, Trp80, and Val270, involving a combination of hydrophobic contacts and occasional hydrogen bonding (Fig. 4G–I).

To assess the stability of these poses when the system was allowed to move, we performed 100-ns molecular dynamics simulations for each complex. Both alkaloids remained in contact with AKT1 throughout the simulations and did not drift significantly from their original location (Supplementary Fig. 7). Ajmalicine exhibited smaller changes in RMSD and modest RMSF values, indicating limited movement relative to the starting pose. The radius of gyration fluctuated only slightly, indicating that the overall shape of the complexes remained compact. Short-lived hydrogen bonds formed at intervals across the trajectories, consistent with the contacts predicted in the docking results.

Taken together, these modelling results indicate that the examined alkaloids are able to associate with AKT1 in a stable manner. Although the simulations cannot confirm inhibition, the predicted interactions

align with the observed reductions in AKT1 expression and protein levels (Fig. 4), offering a reasonable structural explanation for the effects seen in kratom-treated breast cancer cells.

Suppression of Mortalin and modulation of p53 signalling by kratom alkaloids

Clinical analysis based on TCGA datasets showed that HSPA9 (mortalin) is consistently overexpressed in breast carcinoma and its elevated expression correlates with poorer patient survival ($p = 0.01$; Supplementary Fig. 5). Given this clinical association, we examined whether kratom alkaloids influence mortalin expression in breast cancer cells. Treatment with a 0.014 mg/mL alkaloid fraction reduced *HSPA9* (mortalin) transcript abundance and increased *TP53* mRNA levels in both MCF-7 and MDA-MB-231 cells (Fig. 5A, B). Immunocytochemistry further showed a decrease in mortalin protein and a corresponding rise in nuclear p53 signal following alkaloid exposure (Fig. 5C, D; Supplementary Fig. 8), consistent with partial restoration of p53 activity in cells that retain wild-type p53 (e.g., MCF-7).

To explore whether these biochemical changes are structurally compatible with direct ligand engagement, we performed docking analyses using mortalin as the receptor (Figs. 5E-H; Supplementary Fig. 13; Supplementary Table 3). Among the screened alkaloids, speciophylline and mitraphylline showed the highest predicted affinity (–6.5 kcal/mol) (Fig. 4E and 5E-H), forming interactions with residues: Phe262, Asn221, Val219, Arg218, Gln424, Leu228, and Asn221, Thr224, Phe262, and Arg218, respectively, which are in line with the reported mortalin–p53 interface. Ajmalicine ranked next (–6.4 kcal/mol) (Fig. 4E and 5E), engaging a similar subset of residues, including Phe262, Thr224, Asn221, Gln424, and Leu228. Other compounds exhibited weaker or more peripheral contacts. These computational results indicate and predict that several alkaloids can adopt geometrically compatible poses near the mortalin–p53 contact region, although docking alone does not confirm disruption of protein–protein interactions.

We next examined whether the docked poses remained stable under molecular dynamics conditions. Simulations performed for 100 ns showed that both speciophylline and mitraphylline and mortalin complexes maintained low RMSD and RMSF values, a stable radius of gyration, and intermittent hydrogen bonding throughout the trajectory (Supplementary Fig. 9). These results support the structural plausibility of alkaloid association with mortalin and predict the potential of alkaloid kratom to inhibit mortalin–p53 binding.

Alkaloids suppress proliferation (Ki-67) and metastatic Marker Expression (MMP9, MMP3) in breast cancer cells

We next examined whether the cellular effects of kratom alkaloids were reflected in changes to recognised markers of proliferation and metastatic behaviour. In both breast cancer models, MCF-7 and MDA-MB-231, treatment with 0.014 mg/mL alkaloid extract resulted in a significant reduction in MMP9 protein abundance, as evidenced by a decrease in fluorescence signal and corresponding quantitative

analyses (Figs. 6A - B for MCF-7; Figs. 6E - F for MDA-MB-231). A similar trend was observed for MMP3, which showed lowered expression in both cell lines (Supplementary Fig. 10). The same treatment also affected Ki67, a marker tightly linked to proliferative activity. In untreated cultures, Ki67 staining was predominantly nuclear. Following exposure to the alkaloid extract, nuclear Ki-67 intensity dropped substantially (Figs. 6C - D for MCF-7; Figs. 6G - H for MDA-MB-231), in line with the G_2/M accumulation noted earlier. The reduction in Ki67 is consistent with an overall dampening of proliferative drive. Taken together, the coordinated decreases in Ki-67, MMP-9, and MMP-3 reinforce the inhibitory effects of kratom alkaloids on pathways governing proliferation and metastatic potential. These molecular changes align with the previously described phenotypic outcomes, indicating a broader suppression of breast cancer cell aggressiveness.

Discussion

The present study demonstrates that alkaloid-rich extracts of *Mitragyna speciosa* effectively inhibit multiple features of breast cancer cell aggressiveness, including reduced metabolic viability, impaired clonogenic survival, and consistent G_2/M phase accumulation in both MCF-7 and MDA-MB-231 cell lines. One plausible molecular contributor to these effects is the reduction of AKT1 at both the transcriptional and protein levels following alkaloid treatment, given the central role of AKT1 in regulating growth and cell-cycle progression in hormone receptor–positive tumours (33). In MCF-7 cells, where AKT1 signalling is strongly linked to cyclin-D1–dependent proliferation, its suppression aligns well with the observed reduction in proliferative capacity. However, because AKT1 has been reported to restrain cell motility in certain triple-negative cell models, such as MDA-MB-231 (34) (17), the anti-migratory effects seen in this cell line cannot be attributed solely to AKT1 downregulation, suggesting the involvement of additional signaling pathways.

Consistent with proposed broader mechanism, kratom alkaloids treatment significantly reduced cell migration and invasion in both breast cancer models, accompanied by decreased MMP9 and MMP3 protein expressions. MMP9 and MMP3 are matrix-remodelling proteases strongly implicated in breast cancer invasion, stromal degradation, and metastatic dissemination (35) (36). Because their transcription is regulated by multiple upstream signalling pathways, including NF-κB, AP-1, and PI3K/AKT-associated stress signaling (37), the concurrent downregulation of both metalloproteinases suggests modulation of interconnected invasion-related networks rather than regulation by a single upstream effector. This interpretation reconciles the divergent functions of AKT1 in luminal A versus triple-negative cell types and supports a broader model in which alkaloid exposure leads to coordinated suppression of extracellular-matrix remodelling pathways.

In addition to these effects, mortalin (HSPA9) emerges as another regulatory axis influenced by the kratom alkaloids. Mortalin is known to bind wild-type p53 in the cytoplasm, thereby preventing its nuclear accumulation and limiting its tumour-suppressive transcriptional functions (38, 39). Alkaloid treatment reduced mortalin transcript and protein levels while concomitantly increasing nuclear p53 staining. Although nuclear localisation alone does not definitively demonstrate transcriptional reactivation of p53,

this shift is consistent with reduced cytoplasmic sequestration and aligns with previous observations in p53-wild-type models such as MCF-7 (40).

The antiproliferative effects of kratom alkaloids were accompanied by decreased Ki-67 expression, consistent with established relationships between cell-cycle arrest and suppressed proliferative indices in breast cancer (41) (42). Together with the observed G_2/M cell-cycle arrest, these findings fit within a broader framework of suppressed cell-cycle progression. Nevertheless, further studies will be required to determine the extent to which disruption of the mortalin–p53 relationship functionally contributes to antiproliferative phenotypes following alkaloid kratom treatment.

Network pharmacology analyses identified AKT1 and mortalin as prominent predicted targets of the alkaloid subset. Molecular docking and molecular dynamics simulations provided structural support for these predictions. Several alkaloids remained stably positioned within the AKT1 active-site cleft, engaging residues observed in known ligand-bound structures (43). Similarly, other alkaloids interacted with surface regions of mortalin corresponding to its p53-binding domain (44), consistent with previous reports targeting the mortalin–p53 binding for cancer therapy (40, 45). Although computational analyses alone cannot demonstrate direct biochemical inhibition, the persistence of these predicted interactions together with the observed transcriptional, proteomic, and phenotypic changes supports a plausible multi-target mode of action.

Taken together, these findings suggest that *M. speciosa* alkaloids induce multiple molecular alterations that work in concert to shape the overall anticancer cellular response. AKT1 appears to contribute predominantly to the anti-proliferative response in luminal A cells, whereas modulation of the mortalin–p53 axis aligns with the G_2/M arrest observed in both cell lines. Coordinated changes in AKT1, MMP9, MMP3, and the mortalin–p53 relationship are consistent with the observed reduction in proliferation, Ki-67 expression, migration, and invasion across the two breast cancer models. Our data suggest that the observed cellular effects are unlikely to arise from the modulation of a single signaling pathway but instead reflect a broader mechanism of action affecting both proliferative and matrix remodeling pathways. The combined downregulation of AKT1, mortalin, Ki-67, MMP9, and MMP3 integrates well with the biological phenotypes observed in both models, highlighting the multi-level nature of the cellular response to kratom alkaloid exposure (Supplementary Fig. 11). Further studies incorporating pathway-specific perturbations, rescue experiments, and *in vivo* models will be necessary to delineate the relative contribution of each axis and to determine whether individual alkaloids or rational combinations possess translational therapeutic potential.

Conclusion

Breast cancer cells of both luminal A and triple-negative subtypes showed reduced viability and clonogenic growth after exposure to *Mitragyna speciosa* alkaloids. Cell-cycle analysis indicated accumulation at the G2/M phase. At the molecular level, treatment was accompanied by lower AKT1 and mortalin expression, along with increased nuclear localization of p53, indicating altered regulation of

proliferation- and stress-related pathways. In addition, decreased expression of Ki-67, MMP-9, and MMP-3 was observed, consistent with reduced proliferative activity and invasive potential. These findings suggest that *M. speciosa* alkaloids interfere with several regulatory components of breast cancer cells, warranting further validation in in vivo models and mechanistic studies.

Declarations

Ethics approval and consent to participate

Not applicable

Consent for publication

Not applicable

Competing interests

The authors declare no competing interests.

Funding

The research was supported by the Research Organization for Health, National Research and Innovation Agency (BRIN), Republic of Indonesia, through “Rumah Program Vaksin dan Obat” 2025, Project Number: CFJRC-ORK2025-956864516648

Author Contribution

A.N.S. conceptualized the study, designed the experiments, performed bioinformatics, molecular, and cell-based analyses, and wrote the original manuscript draft. D.W.I. conducted molecular analyses, data collection, statistical analysis, interpretation, and wrote the original manuscript draft. S.I.R. contributed to the experimental design and performed molecular and cell culture experiments. A.B. assisted in data collection and experimental validation. G.S., U.R., and G. J. G. provided scientific discussions, manuscript reviews, and revisions. P.A., B., and Y.H. were responsible for sample preparation and extraction processes. N. L. P. I. D. contributed to validation and data curation. M.Y.P. supervised the project, providing overall guidance and overseeing the finalization of the manuscript. All authors have read and approved the final version of the manuscript.

Acknowledgement

The authors would like to express their gratitude to the Research Center for Vaccines and Drugs, Research Organization for Health, and the National Research and Innovation Agency (BRIN) for providing

the research facilities and support. We thank Bionyeri Pty Ltd for providing some of the research consumables. Appreciation is also extended to all members of the BRIN Kratom Research Team for their valuable input and collaboration throughout this study. We would also like to acknowledge Alfa Marzelino for his assistance with the bioinformatics analyses and Nyaris Indra Kuncoro for his assistance with the cell culture experiments.

Data Availability

All data generated or analysed during this study are included in this published article and its supplementary information files. Additional raw data are available from the corresponding author upon reasonable request.

References

1. Barrios CH. Global challenges in breast cancer detection and treatment. Breast. 2022;62(Suppl 1):S3–6.
2. Lukasiewicz S, Czeczelewski M, Forma A, Baj J, Sitarz R, Stanislawek A. Breast Cancer-Epidemiology, Risk Factors, Classification, Prognostic Markers, and Current Treatment Strategies-An Updated Review. Cancers (Basel). 2021;13(17).
3. Yersal O, Barutca S. Biological subtypes of breast cancer: Prognostic and therapeutic implications. World J Clin Oncol. 2014;5(3):412–24.
4. Carvalho E, Canberk S, Schmitt F, Vale N. Molecular Subtypes and Mechanisms of Breast Cancer: Precision Medicine Approaches for Targeted Therapies. Cancers (Basel). 2025;17(7).
5. Ahn JH, Choi SB, Park JM, Kim JY, Park HS, Kim SI, et al. Level of Combined Estrogen and Progesterone Receptor Expression Determines the Eligibility for Adjuvant Endocrine Therapy in Breast Cancer Patients. Cancers (Basel). 2021;13:19.
6. Cheng X. A Comprehensive Review of HER2 in Cancer Biology and Therapeutics. Genes (Basel). 2024;15(7).
7. Lammers SWM, Tjan-Heijnen VCG, Geurts SME, Vriens IJH. Response to letter re: The prognostic and predictive value of the luminal-like subtype in hormone receptor-positive breast cancer: an analysis of the DATA trial. ESMO Open. 2025;10(5):105068.
8. Onder AH. Letter re: The prognostic and predictive value of the luminal-like subtype in hormone receptor-positive breast cancer: an analysis of the DATA trial. ESMO Open. 2025;10(5):105066.
9. Ignatiadis M, Sotiriou C. Luminal breast cancer: from biology to treatment. Nat Rev Clin Oncol. 2013;10(9):494–506.
10. Zhang XH, Giuliano M, Trivedi MV, Schiff R, Osborne CK. Metastasis dormancy in estrogen receptor-positive breast cancer. Clin Cancer Res. 2013;19(23):6389–97.

11. Matsumoto A, Jinno H, Murata T, Seki T, Takahashi M, Hayashida T, et al. Prognostic implications of receptor discordance between primary and recurrent breast cancer. Int J Clin Oncol. 2015;20(4):701–8.
12. Xiong N, Wu H, Yu Z. Advancements and challenges in triple-negative breast cancer: a comprehensive review of therapeutic and diagnostic strategies. Front Oncol. 2024;14:1405491.
13. Miricescu D, Totan A, Stanescu S, Badoiu II, Stefani SC, Greabu C. M. PI3K/AKT/mTOR Signaling Pathway in Breast Cancer: From Molecular Landscape to Clinical Aspects. Int J Mol Sci. 2020;22(1).
14. Khorasani ABS, Hafezi N, Sanaei MJ, Jafari-Raddani F, Pourbagheri-Sigaroodi A, Bashash D. The PI3K/AKT/mTOR signaling pathway in breast cancer: Review of clinical trials and latest advances. Cell Biochem Funct. 2024;42(3):e3998.
15. Havalova H, Ondrovicova G, Keresztesova B, Bauer JA, Pevala V, Kutejova E et al. Mitochondrial HSP70 Chaperone System-The Influence of Post-Translational Modifications and Involvement in Human Diseases. Int J Mol Sci. 2021;22(15).
16. Wu PK, Hong SK, Chen W, Becker AE, Gundry RL, Lin CW, et al. Mortalin (HSPA9) facilitates BRAF-mutant tumor cell survival by suppressing ANT3-mediated mitochondrial membrane permeability. Sci Signal. 2020;13:622.
17. Rao G, Pierobon M, Kim IK, Hsu WH, Deng J, Moon YW, et al. Inhibition of AKT1 signaling promotes invasion and metastasis of non-small cell lung cancer cells with K-RAS or EGFR mutations. Sci Rep. 2017;7(1):7066.
18. Zhang HP, Jiang RY, Zhu JY, Sun KN, Huang Y, Zhou HH, et al. PI3K/AKT/mTOR signaling pathway: an important driver and therapeutic target in triple-negative breast cancer. Breast Cancer. 2024;31(4):539–51.
19. Kaboli PJ, Imani S, Jomhori M, Ling KH. Chemoresistance in breast cancer: PI3K/Akt pathway inhibitors vs the current chemotherapy. Am J Cancer Res. 2021;11(10):5155–83.
20. Zhu Z, Yu W, Fu X, Sun M, Wei Q, Li D, et al. Phosphorylated AKT1 is associated with poor prognosis in esophageal squamous cell carcinoma. J Exp Clin Cancer Res. 2015;34(1):95.
21. Wadhwa R, Takano S, Kaur K, Deocaris CC, Pereira-Smith OM, Reddel RR, et al. Upregulation of mortalin/mthsp70/Grp75 contributes to human carcinogenesis. Int J Cancer. 2006;118(12):2973–80.
22. Yun CO, Bhargava P, Na Y, Lee JS, Ryu J, Kaul SC, et al. Relevance of mortalin to cancer cell stemness and cancer therapy. Sci Rep. 2017;7:42016.
23. Yun CW, Kim HJ, Lim JH, Lee SH. Heat Shock Proteins: Agents of Cancer Development and Therapeutic Targets in Anti-Cancer Therapy. Cells. 2019;9(1).
24. Chopra B, Dhingra AK. Natural products: A lead for drug discovery and development. Phytother Res. 2021;35(9):4660–702.
25. Wang L, Yan Y, Wu L, Peng J. Natural products in non-alcoholic fatty liver disease (NAFLD): Novel lead discovery for drug development. Pharmacol Res. 2023;196:106925.

26. Hossain R, Sultana A, Nuinoon M, Noonong K, Tangpong J, Hossain KH et al. A Critical Review of the Neuropharmacological Effects of Kratom: An Insight from the Functional Array of Identified Natural Compounds. Molecules. 2023;28(21).
27. Bayu A, Rahmawati SI, Karim F, Panggabean JA, Nuswantari DP, Indriani DW et al. An In Vitro Examination of Whether Kratom Extracts Enhance the Cytotoxicity of Low-Dose Doxorubicin against A549 Human Lung Cancer Cells. Molecules. 2024;29(6).
28. Indriani DW, Rahmawati SI, Bayu A, Ahmadi P, Sari AN, Zuraida Z, et al. Serotonin release mediates analgesia via opioidergic system and withdrawal symptoms in chronic kratom extract-treated mice. BMC Complement Med Ther. 2025;25(1):205.
29. Rahmawati SI, Indriani DW, Ningsih FN, Hardhiyuna M, Firdayani F, Ahmadi P, et al. Dual anti-inflammatory activities of COX-2/5-LOX driven by kratom alkaloid extracts in lipopolysaccharide-induced RAW 264.7 cells. Sci Rep. 2024;14(1):28993.
30. Hassan Z, Muzaimi M, Navaratnam V, Yusoff NH, Suhaimi FW, Vadivelu R, et al. From Kratom to mitragynine and its derivatives: physiological and behavioural effects related to use, abuse, and addiction. Neurosci Biobehav Rev. 2013;37(2):138–51.
31. Glaviano A, Foo ASC, Lam HY, Yap KCH, Jacot W, Jones RH, et al. PI3K/AKT/mTOR signaling transduction pathway and targeted therapies in cancer. Mol Cancer. 2023;22(1):138.
32. Li H, Prever L, Hirsch E, Gulluni F. Targeting PI3K/AKT/mTOR Signaling Pathway in Breast Cancer. Cancers (Basel). 2021;13(14).
33. Tsai PJ, Lai YH, Manne RK, Tsai YS, Sarbassov D, Lin HK. Akt: a key transducer in cancer. J Biomed Sci. 2022;29(1):76.
34. Hinz N, Jucker M. Distinct functions of AKT isoforms in breast cancer: a comprehensive review. Cell Commun Signal. 2019;17(1):154.
35. Duffy MJ, Maguire TM, Hill A, McDermott E, O'Higgins N. Metalloproteinases: role in breast carcinogenesis, invasion and metastasis. Breast Cancer Res. 2000;2(4):252–7.
36. Kwon MJ. Matrix metalloproteinases as therapeutic targets in breast cancer. Front Oncol. 2022;12:1108695.
37. Lee CW, Lin CC, Lin WN, Liang KC, Luo SF, Wu CB, et al. TNF-alpha induces MMP-9 expression via activation of Src/EGFR, PDGFR/PI3K/Akt cascade and promotion of NF-kappaB/p300 binding in human tracheal smooth muscle cells. Am J Physiol Lung Cell Mol Physiol. 2007;292(3):L799–812.
38. Wadhwa R, Takano S, Robert M, Yoshida A, Nomura H, Reddel RR, et al. Inactivation of tumor suppressor p53 by mot-2, a hsp70 family member. J Biol Chem. 1998;273(45):29586–91.
39. Kaul SC, Aida S, Yaguchi T, Kaur K, Wadhwa R. Activation of wild type p53 function by its mortalin-binding, cytoplasmically localizing carboxyl terminus peptides. J Biol Chem. 2005;280(47):39373–9.
40. Elwakeel A, Sari AN, Dhanjal JK, Meidinna HN, Sundar D, Kaul SC et al. Mutant p53(L194F) Harboring Luminal-A Breast Cancer Cells Are Refractory to Apoptosis and Cell Cycle Arrest in Response to Mortaparib(Plus), a Multimodal Small Molecule Inhibitor. Cancers (Basel). 2021;13(12).

41. Davey MG, Hynes SO, Kerin MJ, Miller N, Lowery AJ. Ki-67 as a Prognostic Biomarker in Invasive Breast Cancer. Cancers (Basel). 2021;13:17.
42. Finkelman BS, Zhang H, Hicks DG, Turner BM. The Evolution of Ki-67 and Breast Carcinoma: Past Observations, Present Directions, and Future Considerations. Cancers (Basel). 2023;15(3).
43. Truebestein L, Hornegger H, Anrather D, Hartl M, Fleming KD, Stariha JTB, et al. Structure of autoinhibited Akt1 reveals mechanism of PIP(3)-mediated activation. Proc Natl Acad Sci U S A. 2021;118:33.
44. Amick J, Schlanger SE, Wachnowsky C, Moseng MA, Emerson CC, Dare M, et al. Crystal structure of the nucleotide-binding domain of mortalin, the mitochondrial Hsp70 chaperone. Protein Sci. 2014;23(6):833–42.
45. Yoon AR, Wadhwa R, Kaul SC, Yun CO. Why is Mortalin a Potential Therapeutic Target for Cancer? Front Cell Dev Biol. 2022;10:914540.

Figures

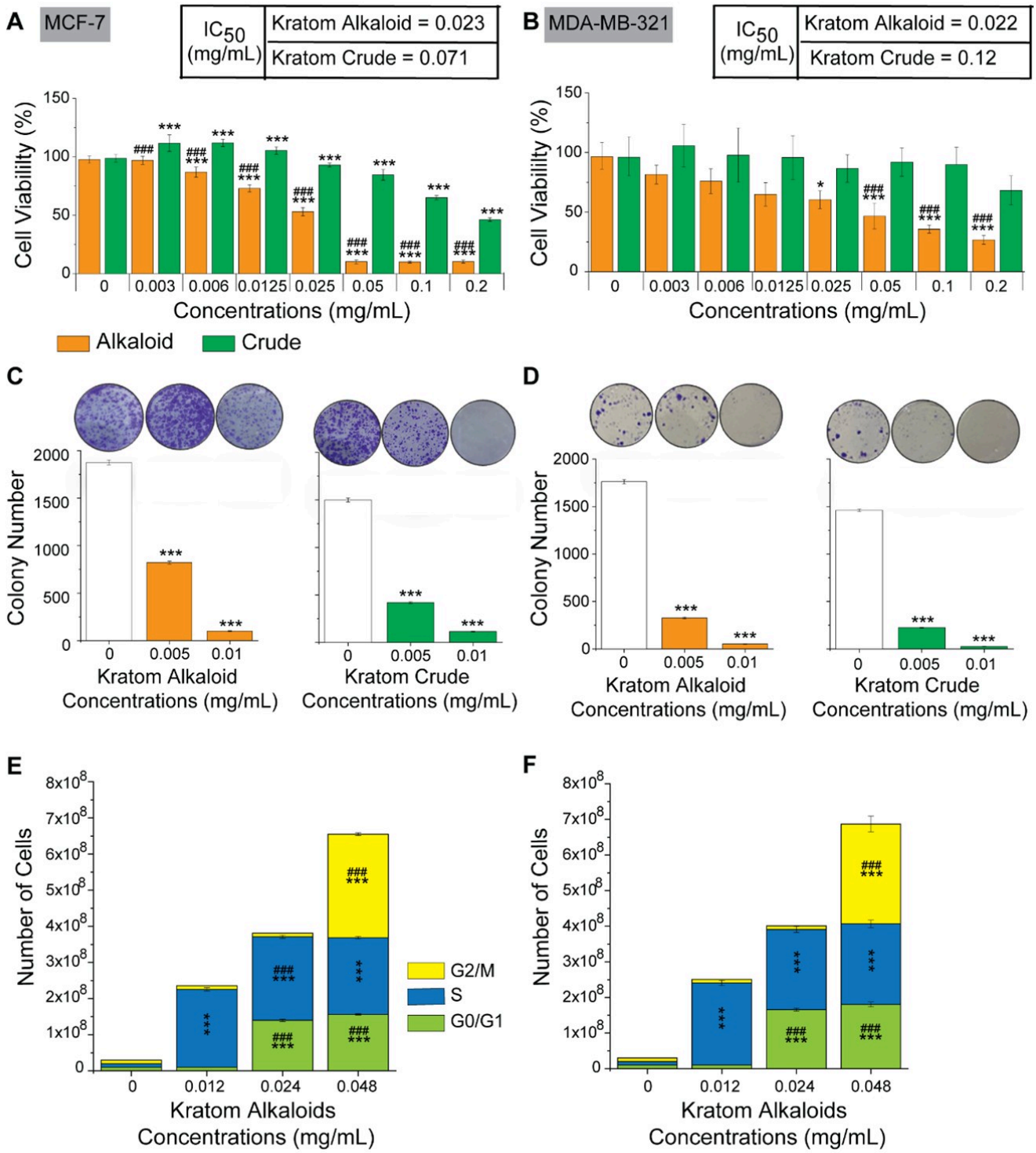

Figure 1

Effects of kratom crude extract (KC) and alkaloid fraction (KA) on cell proliferation and the cell cycle in breast cancer cells. MTT assays of MCF-7 (A) and MDA-MB-231 (B) cells were performed after 48 hours of treatment with the indicated concentrations of KC and KA. Clonogenic assays of MCF-7 (C) and MDA-MB-231(D) cells were conducted following exposure to the specified concentrations of KC and KA. Cell cycle analysis in MCF-7 (E) and MDA-MB-231 (F) cells treated with KA was evaluated after DAPI staining.

Data are expressed as mean ± SD (n ³ 3). * p < 0.05, *** p < 0.001 indicate significant differences compared with the control group (0 mg/mL extract); # p < 0.05, ### p < 0.001 indicate significant differences between KC and KA at the same concentration. Statistical analysis was performed using one-way ANOVA followed by Tukey's post hoc test.

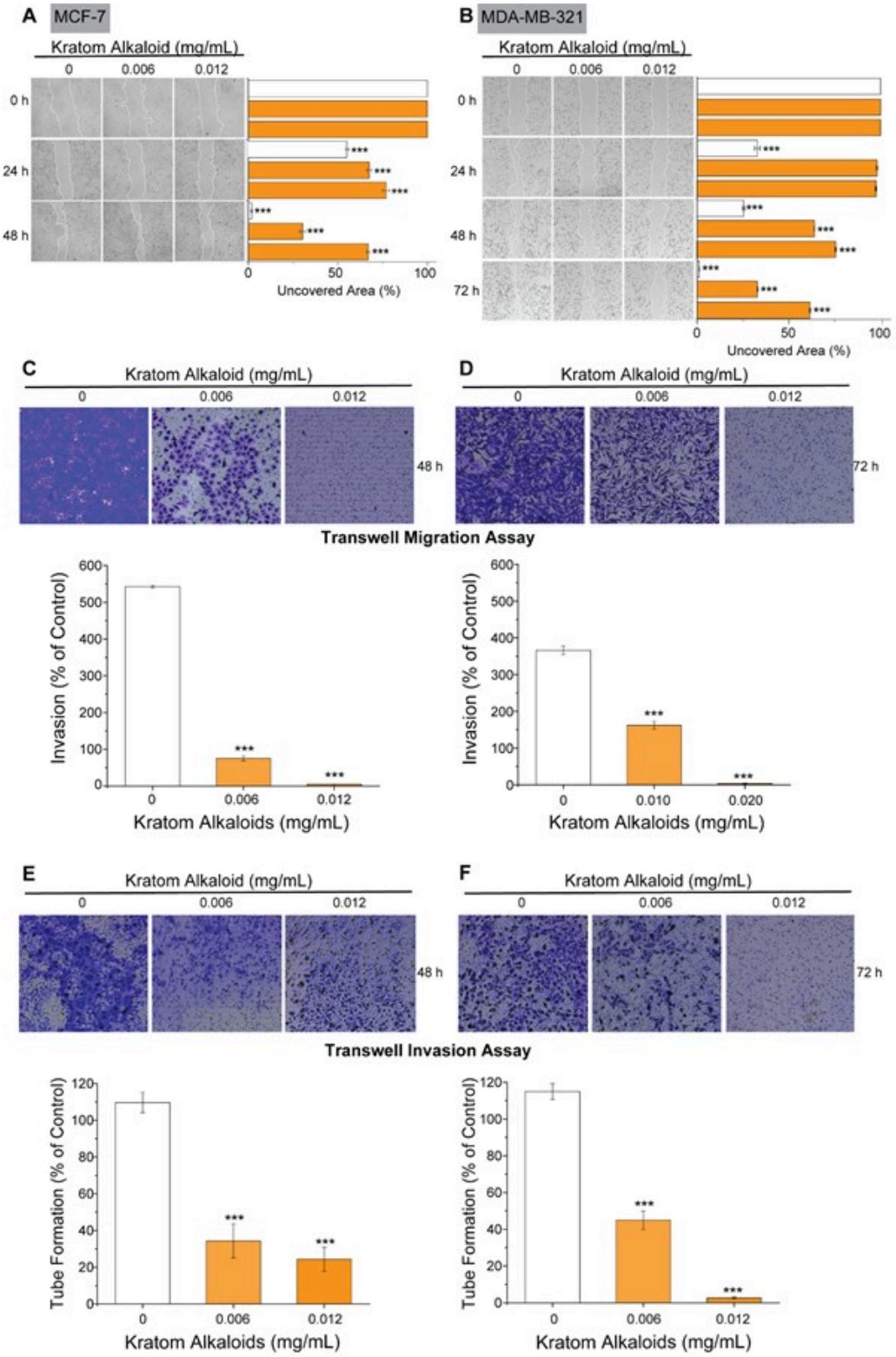

Figure 2

Migration and invasion analysis of MCF-7 and MDA-MB-231 cells following treatment with kratom crude extract and alkaloid fractions. Wound-healing assays were performed at 0, 24, 48, and 72 hours under the indicated treatment conditions of MCF-7 (A) and MDA-MB-231 cells (B). The transwell migration assay shows representative images and quantification of migrated cells in MCF-7 (C) and MDA-MB-231 cells (D). The Matrigel-coated transwell invasion assay presents representative images and quantification of invasive cells in MCF-7 (E) and MDA-MB-231 cells (F). Data are expressed as mean ± SD (n ³ 3). * $p < 0.05$, *** $p < 0.001$ indicate significant differences compared with the control group (0 mg/mL extract). Statistical analysis was performed using one-way ANOVA followed by Tukey's post hoc test.

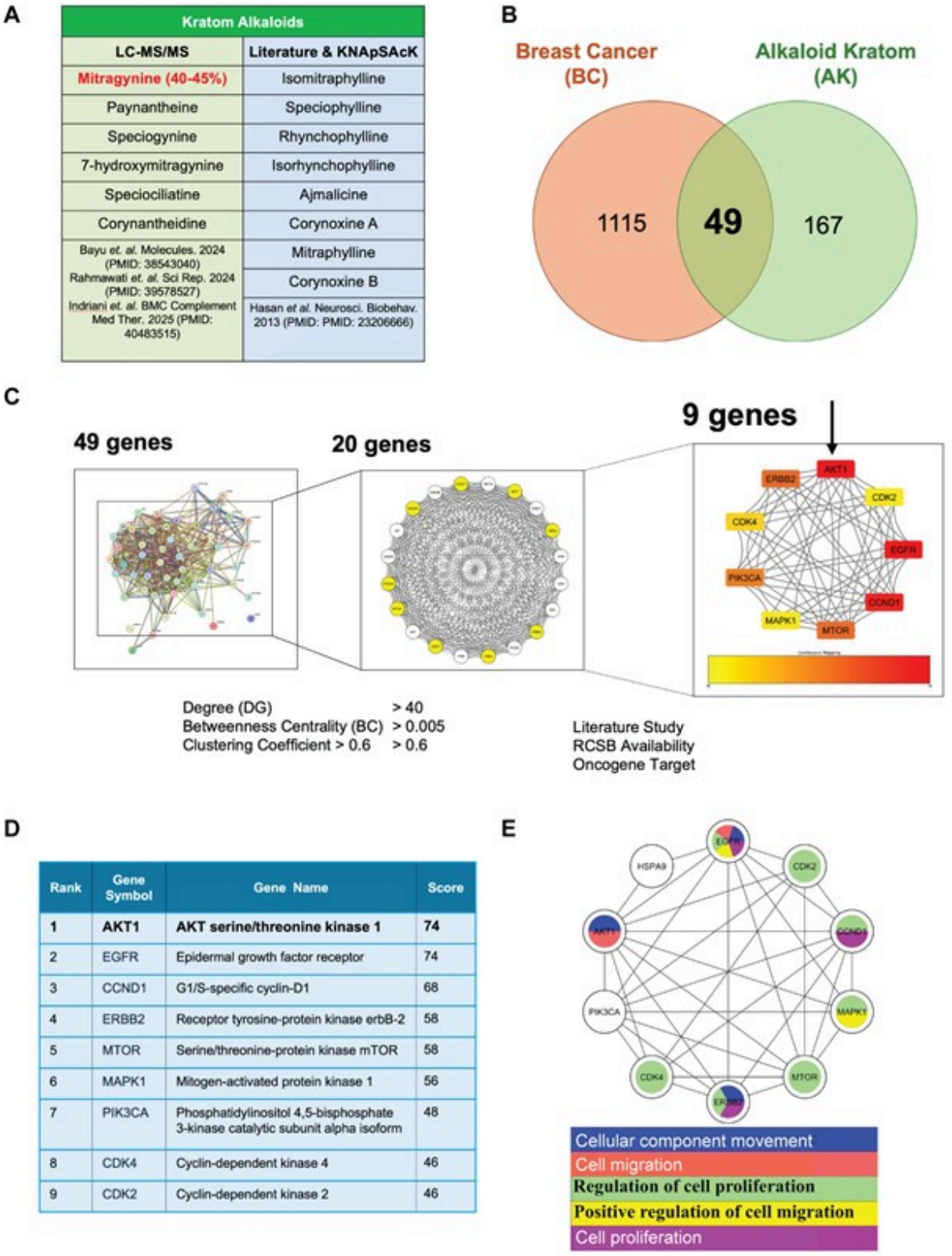

Figure 3

Pharmacological network profile of kratom alkaloids for breast cancer. (A) Alkaloids identified from LC-MS/MS and literature. (B) Venn diagram illustrating the overlap between breast cancer-related genes and kratom target genes. (C–F) Protein–protein interaction (PPI) network, hub gene selection, and functional grouping of major target genes.

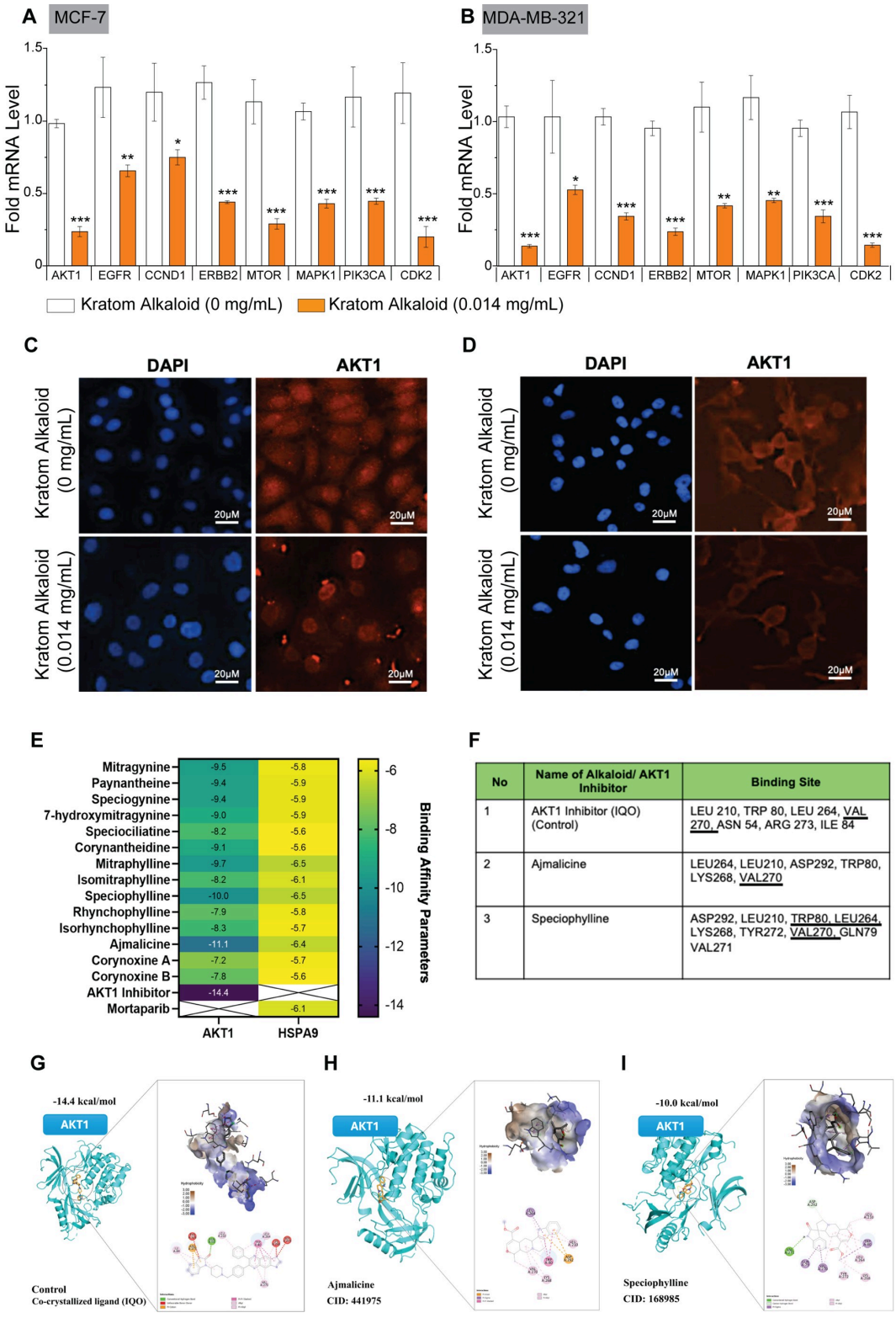

No	Name of Alkaloid/ AKT1 Inhibitor	Binding Site
1	AKT1 Inhibitor (IQO) (Control)	LEU 210, TRP 80, LEU 264, VAL 270, ASN 54, ARG 273, ILE 84
2	Ajmalicine	LEU264, LEU210, ASP292, TRP80, LYS268, VAL270
3	Speciophylline	ASP292, LEU210, TRP80, LEU264, LYS268, TYR272, VAL270, GLN79 VAL271

Figure 4

Effects of kratom alkaloids on AKT1 mRNA and protein expression in breast cancer cells and predicted interactions with AKT1. Quantitative reverse transcription PCR (qRT-PCR) analysis of oncogene expression, including *AKT1, EGFR, CCND1, ERBB2, MTOR, MAPK1, PIK3CA*, and *CDK2*, in MCF-7 (A) and MDA-MB-231 (B) breast cancer cells treated with kratom alkaloids (0.014 mg/mL) compared with untreated controls (0 mg/mL). Gene expression levels are presented as fold changes relative to the

control group. Representative immunofluorescence images showing AKT1 protein expression (red) with DAPI nuclear counterstaining (blue) in MCF-7 (C) and MDA-MB-231 (D) cells following kratom alkaloid treatment. Scale bar: 20 μm. (E) Heatmap illustrating molecular docking scores of major kratom alkaloids against AKT1 and HSPA9 (Mortalin), indicating predicted binding affinities between alkaloids and the target proteins. (F) Identification of key amino acid residues involved in the predicted interactions between AKT1 and selected ligands, including the co-crystallized AKT1 inhibitor (IQO), ajmalicine, and speciophylline. (G–I) Molecular docking visualization of AKT1–ligand complexes, showing binding poses and interaction profiles of AKT1 with the co-crystallized inhibitor IQO (G), ajmalicine (H), and speciophylline (I). Data are expressed as mean ± SD ($n \geq 3$). *$p < 0.05$, **$p < 0.01$, and ***$p < 0.001$ indicate statistically significant differences compared with the control group (0 mg/mL).

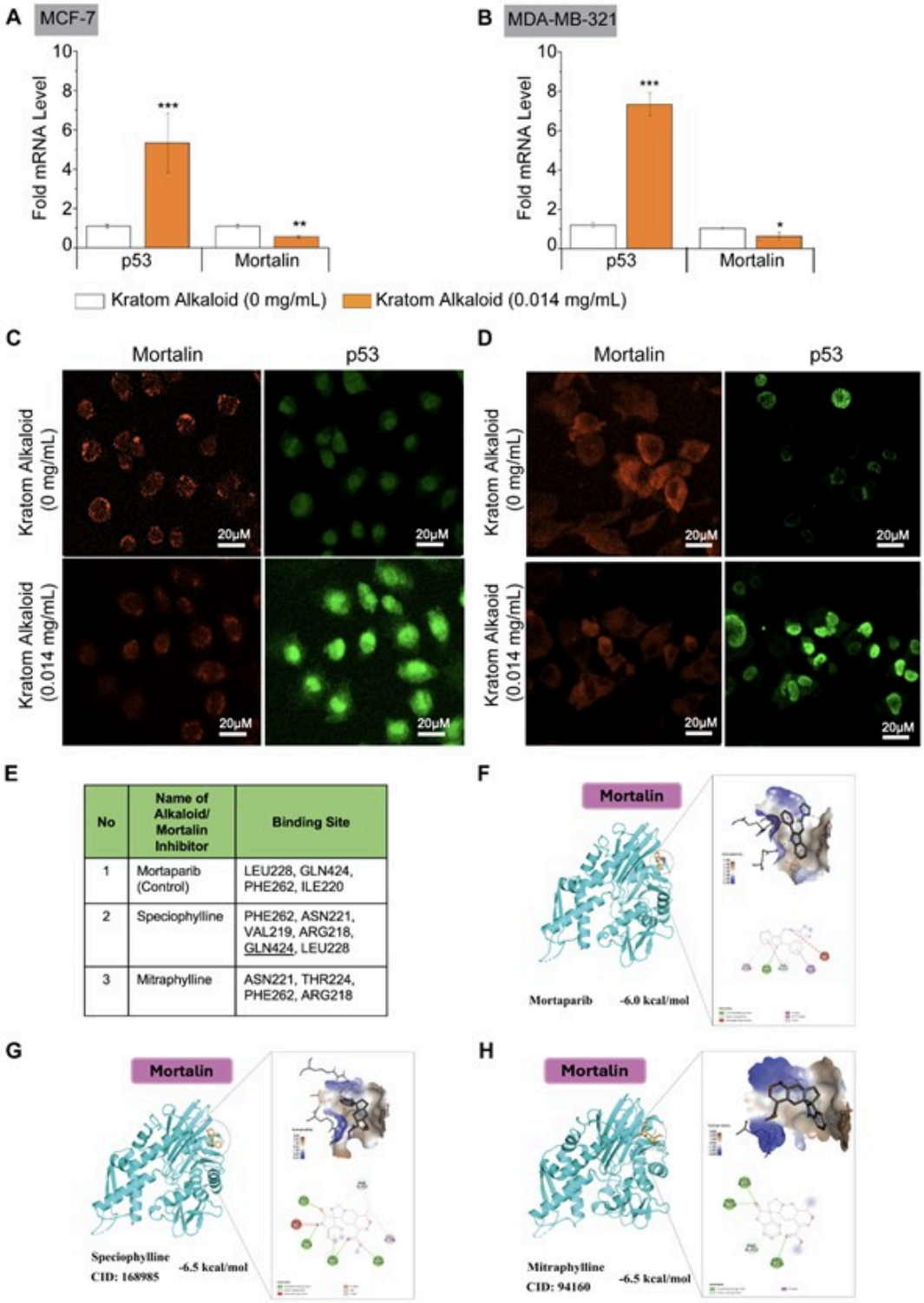

Figure 5

Kratom**alkaloids inhibit mortalin and reestablish p53 signalling.** qRT-PCR analysis of mortalin and p53 expression in MCF-7 (A) and MDA-MB-231 cells (B). Data are expressed as mean ± SD (n ³ 3). * p < 0.05, ** p < 0.01, *** p < 0.001 indicate significant differences compared with the control group (0 mg/mL extract). Statistical analyses were performed using a two-sample t-test in each oncogene, comparing the treatment group to its corresponding control. Immunocytochemistry of mortalin and p53 MCF-7 (C) and

MDA-MB-231 cells (D). (E) Docking score of mortalin–alkaloid complexes. (F-H) Docking visualization of mortalin–alkaloid complexes.

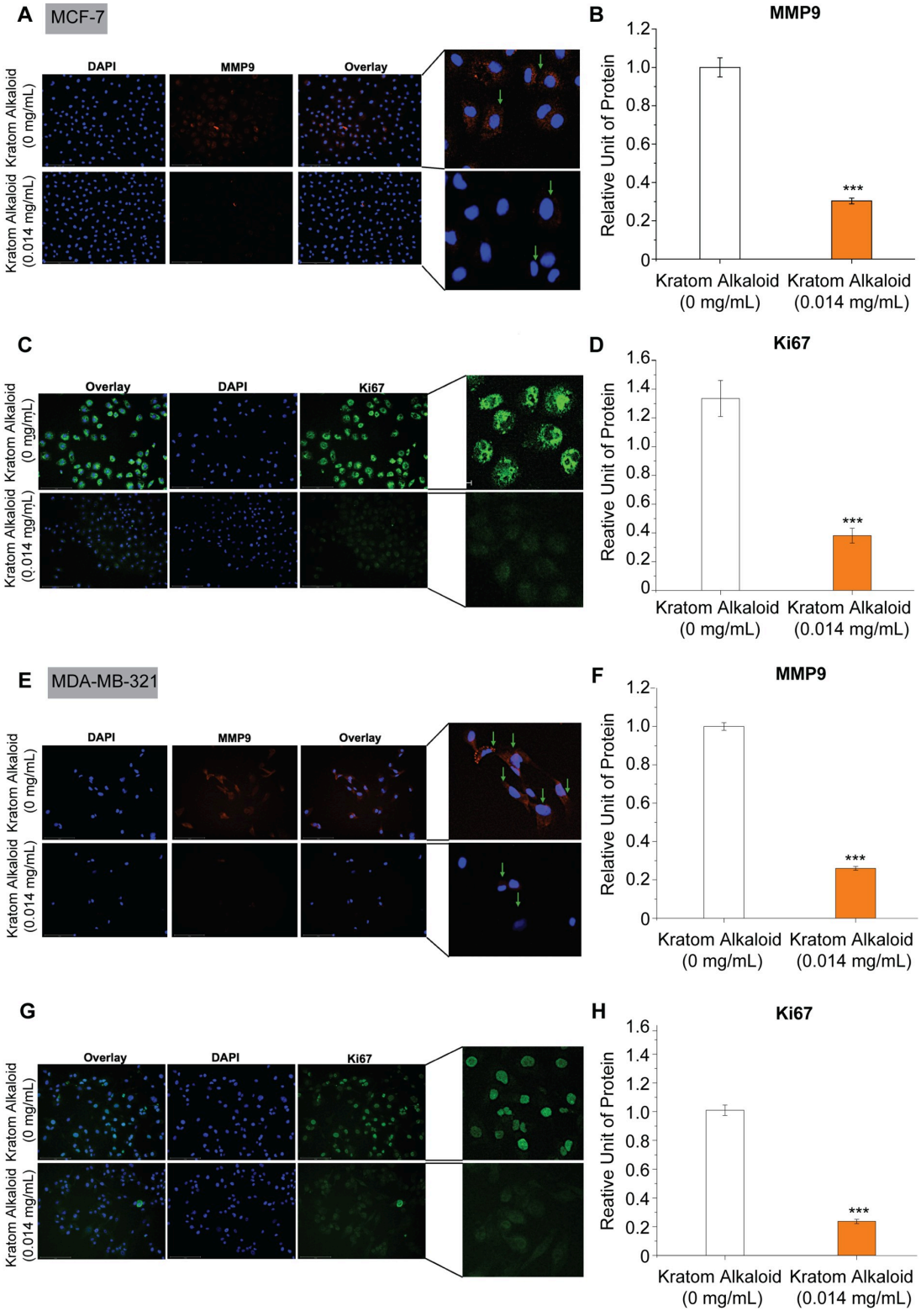

Figure 6

Expression of MMP9 and Ki67 in MCF-7 and MDA-MB-231 cells after kratom alkaloid treatment. (A–B) Immunocytochemistry of MMP9 in MCF-7 cells. (C–D) Immunocytochemistry of Ki67 in MCF-7. (E–F) Immunocytochemistry of MMP9 in MDA-MB-231 cells. (G–H) Immunocytochemistry of Ki67 in MDA-MB-

231. Scale bar: 20 μm. Data are expressed as mean ± SD (n ³ 3). * p < 0.05, ** p < 0.01, *** p < 0.001 indicate significant differences compared with the control group (0 mg/mL extract). Statistical analyses were performed using a two-sample t-test for each oncogene, comparing the treatment group to its corresponding control.

Supplementary Files

This is a list of supplementary files associated with this preprint. Click to download.

- 2.Sarietal2025ManuscriptKratom251219Supplementary.docx